Nanoscale Res Lett (2010) 5:834–838
DOI 10.1007/s11671-010-9570-9

NANO EXPRESS

Self-Organized Ni Nanocrystal Embedded in $BaTiO_3$ Epitaxial Film

F. F. Ge · X. M. Wang · L. H. Cao · J. Li · H. L. Zhang · H. P. Wang · Y. Dai · H. B. Wang · J. Shen · W. D. Wu

Received: 3 January 2010 / Accepted: 25 February 2010 / Published online: 14 March 2010

Abstract Ni nanocrystals (NCs) were embedded in $BaTiO_3$ epitaxial films using the laser molecular beam epitaxy. The processes involving the self-organization of Ni NCs and the epitaxial growth of $BaTiO_3$ were discussed. With the in situ monitoring of reflection high-energy electron diffraction, the nanocomposite films were engineered controllably by the fine alternation of the self-organization of Ni NCs and the epitaxial growth of $BaTiO_3$. The transmission electron microscopy and the X-ray diffraction characterization confirmed that the composite film consists of the Ni NCs layers alternating with the (001)/(100)-oriented epitaxial $BaTiO_3$ separation layers.

Keywords Laser molecular beam epitaxy · Nanocomposite film · Reflection high-energy electron diffraction · Self-organization · Epitaxial growth

F. F. Ge · X. M. Wang · L. H. Cao · J. Li · H. L. Zhang · H. P. Wang · Y. Dai · H. B. Wang · J. Shen · W. D. Wu (✉)
Research Center of Laser Fusion, CAEP, P.O. Box 919-983, 621900 Mianyang, China
e-mail: wuweidongding@163.com; gefangfang@126.com

F. F. Ge
Department of Physics, Tongji University, 20092 Shanghai, China

H. L. Zhang
Laboratory for Magnetism and Magnetic Materials of the Ministry of Education, Physical Science and Technology School, Lanzhou University, 730000 Lanzhou, China

Introduction

The embedding of metal nanocrystals (NCs) in dielectric matrix is of considerable interest for the widely potential application in nonlinear optical device and nano-electronics [1–3]. The properties depend on mainly the size and shape of the nanoparticles, the embedding environment, and so on [4, 5]. However, the controllable fabrication of nanostructure remains the daunting challenge for many deposition methods, including sol–gel [6], atom beam sputtering [7], and pulsed-laser deposition (PLD) [8, 9]. Another attractive method is referred to as a "self-organized" growth, in which the strain force would drive the three-dimensional (3D) island to form in the lattice mismatched growth process [10, 11]. Such "self-organization" growth process has been performed to fabricate the quantum structure in semiconductor devices successfully, such as InAs on GaAs, SiGe on Si [12]. To our knowledge, there is seldom report about the self-organization process of metal NCs in oxide matrix. In this work, the laser molecular beam epitaxy (L-MBE) was used to embed the Ni NCs in the $BaTiO_3$ epitaxial film. The fabrication of the Ni-$BaTiO_3$ nanocomposite system is interesting and significant for both fundamental and application aspects. Such composite films offer an combination of ferroelectric and ferromagnetic characteristics. Furthermore, another important application for Ni-$BaTiO_3$ system is the nanoelectronics such as the base-metal-electrode multilayered ceramic capacitors (BME-MLCC) [13].

Experimental

The Ni:$BaTiO_3$ epitaxial films were prepared on $SrTiO_3$ (001) substrate with $BaTiO_3$/$SrTiO_3$ buffer layers by

Table 1 The experimental parameters for the Ni-$BaTiO_3$ film fabrication

Background vacuum	$\sim 3 \times 10^{-6}$ Pa
Working vacuum	$\sim 5 \times 10^{-5}$ Pa
Substrate	$SrTiO_3$ (001)
Substrate temperature	$\sim$650°C
Target	$BaTiO_3$ purity > 99.9%
	Ni purity > 99.9%
Annealing condition	650°C, 30 min
	10 Pa O_2 pressure
Laser energy density	248 nm, 2–3 J/cm^2
Laser pulse frequency	1 Hz for $BaTiO_3$ deposition
	1 Hz for $SrTiO_3$ deposition
	2 Hz for Ni deposition

L-MBE. The experimental parameters were listed in detail in Table 1. The deposition process involved a number of pulses on the Ni target in ultra high vacuum, followed by the epitaxial growth of $BaTiO_3$ layer. After the completion of every $BaTiO_3$ layer,the sample was annealed about 30 min in the oxygen ambient pressure. Such procedure was repeated up to 8 times to grow 300-nm-thick composite film. During the deposition process, the in situ reflection high-energy electron diffraction (RHEED) monitoring was performed in anti-Bray condition using 25-keV electron beam under a grazing incidence of 1^0–3^0 toward the surface. The microstructure and crystallinity of the nanocomposite films were characterized by transmission electron microscopy (TEM) and X-ray diffraction (XRD), respectively.

Results and Discussion

Figure 1a–d recorded the variation of RHEED pattern along the [100] azimuth in the self-organization course of Ni NCs on $BaTiO_3$ (001) surface. With the increasing of Ni deposition pulses, the streak pattern of $BaTiO_3$ disappears gradually, while the spot pattern of Ni NCs becomes dominant. It is considered that the Ni islands formed on $BaTiO_3$ (001) surface, giving rising to bulk diffraction spots. Due to the large lattice mismatch between Ni and $BaTiO_3$ (>9%), the in-plane lattice of Ni is subjected to large tensile strain to match the in-plane lattice of $BaTiO_3$ at the initial stage. With the continuing deposition, the increasing strain energy is reduced by the formation of 3D islands with the enlargement surface. Therefore, the strain acts as a source of driving force for the self-organization of Ni NCs [10, 11]. In such growth process, the lattice of Ni NCs was relaxed to the value of Ni metal bulk. The curves II and III in Fig. 1e represent the diffraction intensities along the horizontal spacing and the vertical spacing,

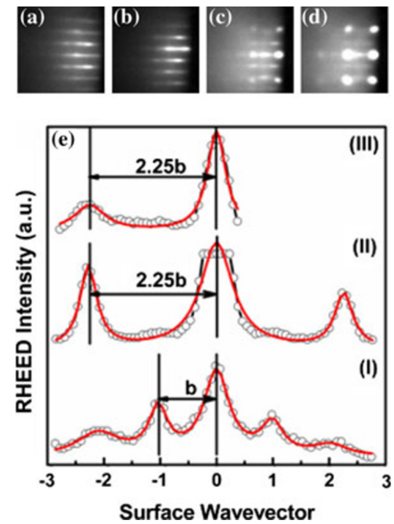

Fig. 1 Evolution of RHEED patterns along the <100> azimuth during the self-organized of Ni NCs process: **a** $BaTiO_3$ surface; **b** 100 pulses Ni; **c** 300 pulses Ni; **d** 600 pulses Ni; **e** The intensity spacing scan for Fig. 1c: *Streak horizontal line* scan (I), *spot horizontal line* scan (II), and *spot vertical line* scan (III)

respectively, for Fig. 1c. If defining the distance between the (0 0), (1 0) $BaTiO_3$ diffraction orders as b shown in curve I, both the horizontal distance and the vertical distance for the Ni bulk diffraction spots equal to 2.25b. This corresponds in real space to a lattice constant of 3.55 Å in cubic structure, close to the crystal structure of bulk Ni metal (3.52 Å) [14]. As well, the same crystal structure for Ni NCs was obtained according to the RHEED pattern along the [110] azimuth. From the patterns along the [100] and [110] azimuths, it demonstrates that the Ni NCs maintain the (001) orientation with in-plane Ni NCs/$BaTiO_3$ epitaxial relationships of $[200]_{Ni}||[100]_{BTO}$ and $[220]_{Ni}||[110]_{BTO}$ during the growth process in 650°C.

The RHEED intensity variation during the $BaTiO_3$ growth on Ni NCs layer is displayed in Fig. 2. The inserts

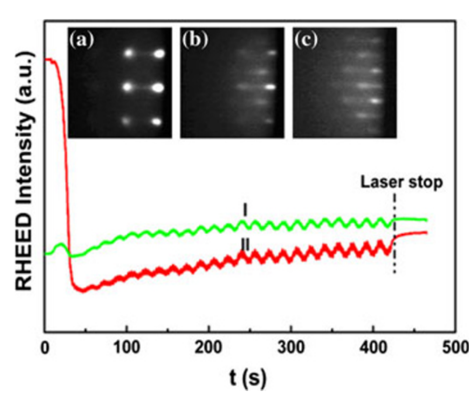

Fig. 2 RHEED intensity oscillations recorded on spot (*curve I*) and streak (*curve II*), respectively, during the $BaTiO_3$ epitaxial growth. The inserts are the RHEED patterns collected at 10, 30, and 50 s

show that the spotty RHEED pattern transforms to the streaky pattern at the initial stage, indicating the recovering of two-dimensional $BaTiO_3$ interface for the subsequent growth. Then, the overall RHEED intensity is enhanced and presents a strong oscillation behavior. It is evident that the $BaTiO_3$ separation layer continued to grow in a layer-by-layer growth mode with the improving of surface smoothness. The appearance of RHEED intensity oscillation provided an effective way for controlling the accurate thickness of separation layer. Figure 3 is the cross-sectional TEM image of Ni:$BaTiO_3$ nanocomposite film. In combination with the TEM result, it was determined that one period of oscillation corresponded to the growth of three $BaTiO_3$ unit cells. The $BaTiO_3$ separation layers were grown repeatedly in perfect layer-by-layer mode on the irregular interface of strained NCs layers, which smoothed the irregular growth front formed in the self-assembled process of Ni NCs and provided a flat substrate for the next strained Ni NCs layer. As Fig. 3 shows, the nanocomposite film consists of eight Ni NCs layers alternating with $BaTiO_3$ separation layers. The sizes of Ni nanocrystals were estimated in the range from 3 to 5 nm. And the $BaTiO_3$ separation layers have the uniform thickness of 30 nm or so. This confirms that the Ni NCs were embedded in $BaTiO_3$ matrix, by the alternating of Ni NCs self-organization process and $BaTiO_3$ epitaxial growth. Since the RHEED pattern is very sensitive to the surface microstructure [15–17], the microstructure and the period of such quantum dot superlattice can be engineered with the in situ monitoring of RHEED.

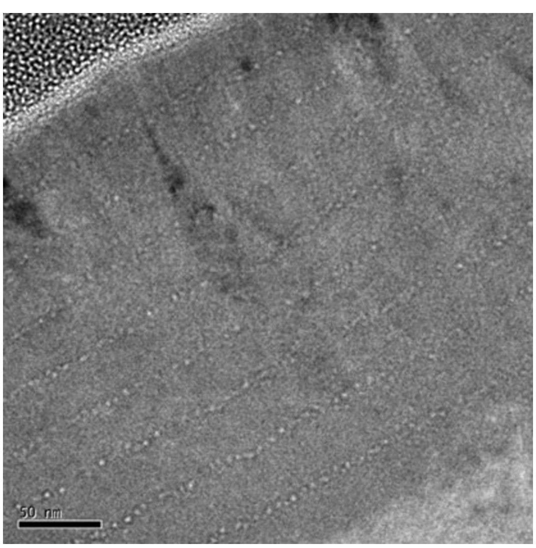

Fig. 3 The cross-sectional TEM image of Ni:$BaTiO_3$ nanocomposite film. It consists of eight Ni NCs layers alternating with $BaTiO_3$ separation layers

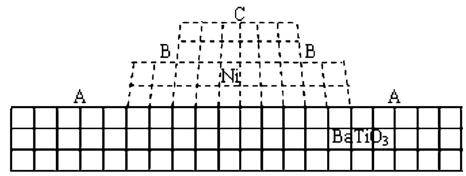

Fig. 4 A schematic diagram of a strained Ni NCs on flat $BaTiO_3$ surface showing the variation of in-plane lattice strain occurring near the growth surface

To identify the growth mechanism of the nanocomposite film, a simple schematic cross-sectional view of Ni NCs layer shown in Fig. 4, with a dislike Ni island strained on the $BaTiO_3$ matrix. After the relaxation of lattice strain for Ni NCs, the in-plane lattice of Ni on region B is stretch near to that of $BaTiO_3$, whereas the in-plane lattice of Ni on region C is relaxed to that of bulk Ni metal. The average in-plane lattice strain at the island surface (region B) is less than the region C away from the island, thus the layer is considered to be uniformly strained. If further growth of $BaTiO_3$ layer, the lattice of the $BaTiO_3$ layer is then distorted above region C, while it is less of distortion above region A ($BaTiO_3$ natural surface) and region B. The epitaxial growth of $BaTiO_3$ in layer-by-layer mode occurs more rapidly above region A and region B with less lattice strain, then forms an atomically flat interface for the subsequent epitaxial growth [18, 19]. Only the relaxation of lattice strain above the well-developed 3D Ni islands is significant, while above the other islands, the strain relaxation is less. Therefore, the 2D growth of $BaTiO_3$ was sustained although the local growth was perturbed by the Ni islands.

Figure 5 compares the structural characterizations of the pure $BaTiO_3$ epitaxial film and the Ni:$BaTiO_3$ nanocomposite films by XRD. Besides the (00 *l*) peaks for the $SrTiO_3$ substrate, Fig. 5a consists of two peaks corresponding to $BaTiO_3$ (001) and $BaTiO_3$ (002), respectively, meaning a single phase in the pure $BaTiO_3$ film. In Fig. 5b and c, the observed systematic shift of the (00 *l*) peaks toward to the lower diffraction angles indicates an increasing of the out-of-plane parameter of $BaTiO_3$ due to the embedding of Ni NCs. The elongating of the out-of-plane lattice is caused by the large compressive strain at the Ni:$BaTiO_3$ interface for the in-plane lattice match. The stronger strain was introduced for the higher Ni NCs concentration with the more obvious shift of the (00 *l*) peaks in Fig. 5c. Furthermore, the extra(*h*00)peaks exhibit in Fig. 5b and c, which is a typical polydomain pattern containing the *c* domains with the *c* axis normal to the surface and the *a* domains with the *a* axis normal to the surface. The domain formation in $BaTiO_3$ epitaxial films is a mechanism that relaxes the total strain energy as a result

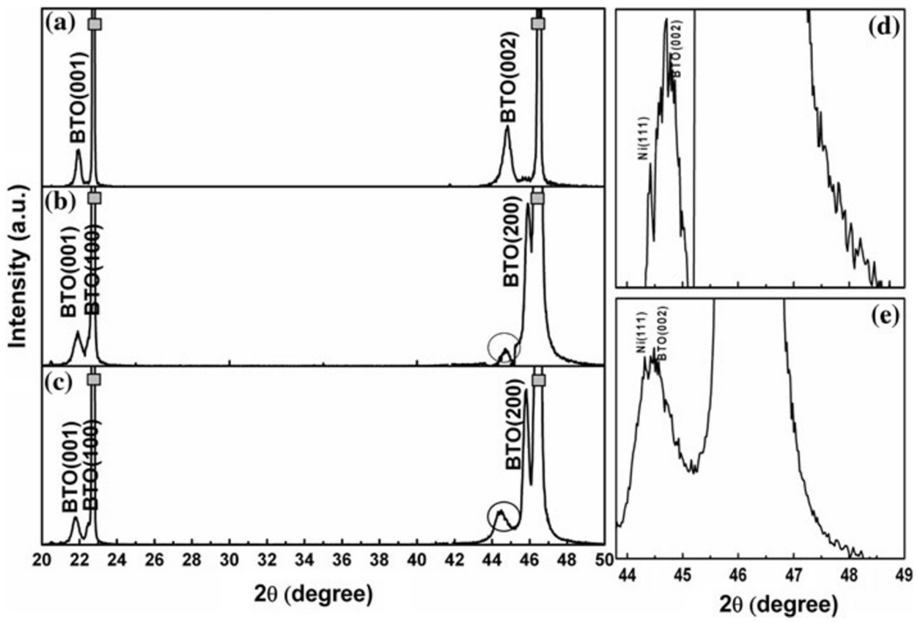

Fig. 5 XRD θ-2θ scans of $BaTiO_3$ film, *filled square* correspond to diffraction peaks from $SrTiO_3$ (001) substrates. **a** pure $BaTiO_3$ film; **b** Ni: $BaTiO_3$ nanocomposite film (300 Ni pulses per layer); **c** Ni: $BaTiO_3$ nanocomposite film (600Ni pulses per layer); **d** an expand view around the 002 $BaTiO_3$ peak with the *circle* label in Fig. 5b; **e** an expand view around the 002 $BaTiO_3$ peak with the *circle* label in Fig. 5c

of the great lattice mismatch [20]. The angles between the surface normal [001] of (001) oriented domains and [100] of (100)-oriented domains is defined as α angle, $\alpha = \{2\arctan(c/a)–90°\}$, where *a* and *c* denote the lattice parameters of the *a* and *c* axes [21]. The total internal angles of *a/c* domains were estimated to be approximately 1.19° and 1.34° for Fig. 5b and c, respectively. Both the values are larger than the theoretical value for the strain-relaxed $BaTiO_3$ powder (0.7°) [22], which illustrates that the c/a/c/a polytwin relieved the internal strain only partially. The XRD characterization confirmed the RHEED result that the epitaxial growth of $BaTiO_3$ was not hindered by the embedding of Ni NCs. However, the strain from the lattice mismatch between Ni and $BaTiO_3$ altered the microstructure of such nanocomposite film.

Magnifying the labeled broad peak, a weak peak was observed beside the $BaTiO_3$ (002) peak shown as the inserts in Fig. 5d and e, which was supposedly the Ni (111) peak. In comparison with the in situ RHEED results, there is a transformation of the preferred out-of-plane orientation for Ni NCs from $[200]_{Ni}||[100]_{BTO}$ to $[111]_{Ni}||[100]_{BTO}$ after annealing. The fcc metal tends to exhibit preferential crystallographic orientation with (111), its closet packed plane, achieving minimum surface energy. The Ni NCs were speculated to remain metallic, which may be attributed to be well protected by the $BaTiO_3$ separation layer. Moreover, Jiang et al. found that oxygen atoms in NiO intermediate layer migrated to the $BaTiO_3$ layer at 800°C [23]. Those results suggest that the co-exist system of metal and orientation-preferred ferroelectric oxides was available by the self-organized growth of metal NCs in ferroelectric oxides.

Conclusion

In summary, the Ni NCs formed in the epitaxial $BaTiO_3$ film by L-MBE. The alternate growth of Ni NCs layer and epitaxial $BaTiO_3$ film was well controllable for the desired quality by the monitoring of RHEED. For the large lattice mismatch between Ni and $BaTiO_3$, the strain drived the self-organization growth of Ni NCs. And the $BaTiO_3$ remained the layer-by-layer growth on the strained Ni NCs layer. The strain was relaxed only partially by the emergence of the (001)/(100) polydomain structure in the $BaTiO_3$ epitaxial film with the elongating of *c* axis.

References

1. V. Keibig, M. Vollmer, Optical Properties of Metal Clusters (Springer, Berlin, 1995)
2. D. Ricard, P. Roussignol, C. Flytzanis, Opt. Lett. **10**, 511 (1985)
3. Z. Liu, C. Lee, V. Narayanan, G. Pei, E.C. Kan, IEEE Trans. Electron Device **49**, 1606 (2002)
4. H.B. Liao, R.F. Xiao, J.S. Fu, R. Yu, G.K.L. Wong, P. Sheng, Appl. Phys. Lett. **70**, 1 (1996)
5. K.L. Kelly, E. Coronado, L.L. Zhao, G.C. Schatz, J. Phys. Chem. B **107**, 668 (2003)
6. G. De, L. Tapfer, M. Catalano, G. Battaglin, F. Caccavale, F. Gonella, P. Mazzoldi, R.F. Haglund, Appl. Phys. Lett. **68**, 3820 (1996)
7. Y.K. Mishra, S. Mohapatra, D. Kabiraj, B. Mohanta, N.P. Lalla, J.C. Pivin, D.K. Avasthi, Scripta Mater. **56**, 629 (2007)

8. W.T. Wang, G. Yang, W.D. Wu, Z.H. Chen, J. Appl. Phys. **94**, 6837 (2003)
9. W.D. Wu, Y.J. He, F. Wang, Z.H. Chen, Y.J. Tang, W.G. Sun, J. Cryst. Growth **289**, 408 (2006)
10. H. Drexler et al., Phys. Rev. Lett. **73**, 2252 (1994)
11. J.Y. Marzin et al., Phys. Rev. Lett. **73**, 716 (1994)
12. J. Tersoff, C. Teichert, M.G. Lagally, Phys. Rev. Lett. **76**, 1675 (1996)
13. Y.C. Huang, S.S. Chen, W.H. Tuan, J. Am. Ceram. Soc. **90**, 1438 (2007)
14. M. Yousuf, P.C. Sahu, H.K. Jajoo et al., J. Phys. F **16**, 373 (1986)
15. R.T. Brewer, H.A. Atwater, J.R. Groves, P.N. Arendt, J. Appl. Phys. **93**, 205 (2003)
16. J. Zhu, X.H. Wei, Y. Zhang, Y.R. Li, J. Appl. Phys. **100**, 104106 (2006)
17. X.H. Wei, Y.R. Li, J. Zhu, Y. Zhang, Z. Liang, W. Huang, J. Phys. D Appl. Phys. **38**, 4222 (2005)
18. J.Y. Yao, T.G. Andersson, G.L. Dunlop, J. Appl. Phys. **69**, 2226 (1991)
19. F. Turco, J.C. Guillaume, J. Massies, J. Crystal. Growth **88**, 282 (1988)
20. S.P. Alay, A.S. Prakash, S. Aggarwal, P. Shuk, M. Greenblatt, R. Ramesh, A.L. Roytburd, Scripta Mater. **39**, 1435 (1998)
21. R.H. Buttner, E.N. Maslen, Acta Crystallographica B **48**, 764 (1992)
22. C. Kittel, Solid State Commun. **10**, 119 (1992)
23. J.C. Jiang, E.I. Meletis, Z. Yuan, J. Liu, J. Weaver, C.L. Chen et al., J. Nano Res. **1**, 59 (2008)